

Impact identification and localization using a sample-force-dictionary – General Theory and its applications to beam structures

Daniel Ginsberg* and Claus-Peter Fritzen

*University of Siegen, Department of Mechanical Engineering, Paul-Bonatz-Strasse 9-11,
57076 Siegen, Germany*

(Received April 28, 2015, Revised July 12, 2015, Accepted January 18, 2016)

Abstract. Monitoring of impact loads is a very important technique in the field of structural health monitoring (SHM). However, in most cases it is not possible to measure impact events directly, so they need to be reconstructed. Impact load reconstruction refers to the problem of estimating an input to a dynamic system when the system output and the impulse response function are usually known. Generally this leads to a so called ill-posed inverse problem. It is reasonable to use prior knowledge of the force in order to develop more suitable reconstruction strategies and to increase accuracy. An impact event is characterized by a short time duration and a spatial concentration. Moreover the force time history of an impact has a specific shape, which also can be taken into account. In this contribution these properties of the external force are employed to create a sample-force-dictionary and thus to transform the ill-posed problem into a sparse recovery task. The sparse solution is acquired by solving a minimization problem known as basis pursuit denoising (BPDN). The reconstruction approach shown here is capable to estimate simultaneously the magnitude of the impact and the impact location, with a minimum number of accelerometers. The possibility of reconstructing the impact based on a noisy output signal is first demonstrated with simulated measurements of a simple beam structure. Then an experimental investigation of a real beam is performed.

Keywords: impact identification; load reconstruction; ill-posed and inverse problem; sparse recovery; simultaneously impact localization and identification

1. Introduction

The knowledge of the external loads is of great interest in many fields of structural analysis, such as structural health monitoring (SHM), assessment of damage after extreme events or prediction of the remaining useful lifetime of the investigated structure. Impact loads are of particular concern as adverse impact events can cause degradation and breakdown of the structure or its components. For example, debris flying from the runway can cause damage of composite aeronautical structures (Abrate 2005) or a boat collision with offshore structures may harm the structural integrity (Li *et al.* 2014). The information of the size of an impact in combination with the impact location is useful to make a statement about a potential damage and its extent. However,

*Corresponding author, Professor, E-mail: daniel.ginsberg@uni-siegen.de

a direct measurement of external impacts might be difficult due to some physical or economical limitations. For instance, the impact location is unknown in general and debar an optimal sensor placement for direct measurement. In reality, impact loads are reconstructed by using measured structural responses induced by these impact excitations. Usually numerous sensors are employed to capture the dynamic behavior of the structure, such as acceleration, velocity or strain. The reconstruction process generally results in an inverse problem, where the structural properties and responses are known while the excitation needs to be determined. This inverse problem can be considered as mathematically ill-posed in most cases, which means that either the existence, the uniqueness or the stability of the solution is violated (Stevens 1987, Jacquelin *et al.* 2003, Inoue *et al.* 2001). If this inversion can be done, the structure itself becomes its own force sensor (Klinkov and Fritzen 2007).

In order to overcome the ill-posed problem several studies have been carried out and a considerable amount of literature has been published on this topic. Generally, the reconstruction of an impact load by means of structural responses consists of two separate subsequent steps: 1) localization of the impact and 2) estimation of the impact size respectively of the impact force history. To locate the position where the impact is applied, the stress waves induced by an impact can be used in a joint time-frequency analysis, for instance (Gaul and Hurlebaus 1998). To estimate the force history, the most straightforward and various employed method is deconvolution, either in frequency domain or in time domain (Doyle 1984, Chang and Sun 1989). Diverse regularization and relaxation techniques have been used to solve the ill-posed problem of deconvolution, often involving a least squares optimization process. In this case, the relation between an impact force and structural responses needs to be determined by a structural model. Additionally the location of the impact force is assumed to be known in advance. In recent years, approaches using neural networks have shown the capability to identify simultaneously location and magnitude of an impact (Jones *et al.* 1997). These techniques require an intensive training of the network by collecting numerous impact test data sets. An alternative identification strategy based on system optimization theory also yield simultaneous estimation of location and force history (Park *et al.* 2009). Here, a filter algorithm which compares estimated outputs from system model with the measured ones is applied. Yan and Zhou (2009) proposed a genetic algorithm (GA) for impact detection, representing the impact load by a set of parameters, thus the identification problem becomes a parameter estimation problem (Yan and Zhou 2009). Torres-Arredondo and Fritzen (2012) convert the identification problem into a pattern recognition task. A combination of time-frequency analysis, auto-associative neural networks for data-driven system modeling and Gaussian processes are employed to automate the identification procedure. Ginsberg and Fritzen (2014) introduced a reconstruction methodology, which take the specific temporal and spatial properties of an impact load into account and is therefore capable of applying sparse recovery algorithms to the ill-posed problem.

The present work may be regarded as direct extension of (Ginsberg and Fritzen 2014), here the specific force history shape of an impact is additionally considered. Thus, more precise and more robust solutions can be obtained. The proposed reconstruction strategy identifies the impact location and the impact force history, simultaneously. This contribution is structured as follows: Section 2 briefly discusses the general problem of impact reconstruction and explains how it can be transformed to a sparse identification problem. In Section 3, the applied approach for solving the sparse reconstruction problem is introduced. The capability of this methodology is demonstrated by means of a simulation study on a simple beam structure in Section 4, which also addresses the potential error sources and displays the corresponding reconstruction deviations. An

experimental investigation in Section 5 validates the proposed identification strategy. Finally, concluding remarks are presented in Section 6.

2. Problem

External forces acting on a structure will cause dynamic responses of this structure such as acceleration, velocity or strain. In general these responses can easily be measured by appropriate sensors. In cases where the system can be considered to be linear during the excitation process, the responses $\mathbf{y}(t) \in R^r$ of the system are linked to the external forces $\mathbf{u}(t) \in R^f$ in the time continuous case by the linear convolution integral

$$\mathbf{y}(t) = \int_0^t \mathbf{h}(t - \tau) \mathbf{u}(\tau) d\tau \tag{1}$$

where $\mathbf{h}(t) \in R^{r \times f}$ denotes a matrix containing the impulse response functions (IRF) $h_{i,j}$, r represents the number of measured responses and f the number of force input positions. It is assumed that $\mathbf{u}(t) = \mathbf{h}(t) = \mathbf{y}(t) = \mathbf{0}$ for $t < 0$. The IRF $h_{i,j}$ describes the dynamic behaviour of the structure, more precisely the transmission of an external force applied at a discrete input position $j = 1, 2, \dots, f$, to the structural responses at output position $i = 1, 2, \dots, r$ (e.g., compare input-output transmission in Fig. 4). In a discrete time domain $t = k\Delta t$ ($k = 0, 1, 2, \dots, n$), the convolution integral becomes an convolution sum

$$\mathbf{y}_k = \sum_{i=0}^k \mathbf{h}_i \cdot \mathbf{u}_{k-i} \tag{2}$$

Here, $\mathbf{h}_i \in R^{r \times f}$, are the so-called Markov parameters.

When the time history and the location of the external forces in addition to the IRF are known the system responses can simply be calculated by solving Eq. (1) or Eq. (2). However, generally the external force respectively the input to the system is unknown and the structural responses are determined by (noisy) measurements.

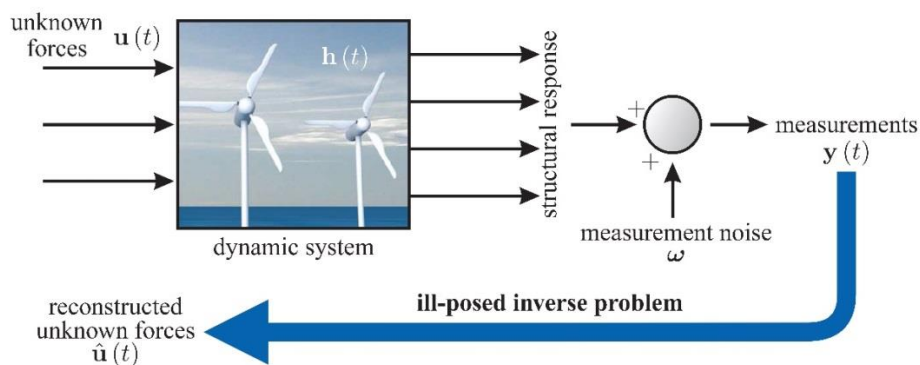


Fig. 1 The problem of force/impact identification

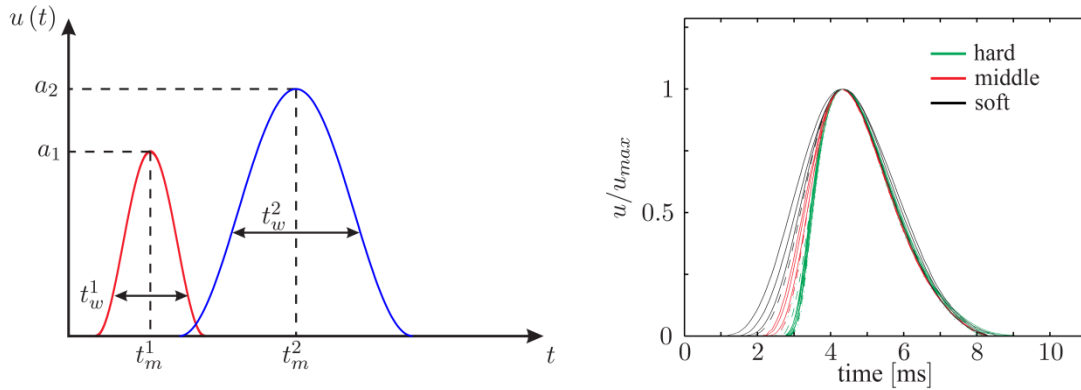


Fig. 2 Force history of an impact, left: general representation, right: normalized experimental records from impacts with different hardness of the colliding bodies

Then the problem of estimating the time history of the forces becomes a deconvolution problem. It is obvious that the IRF or the Markov parameters should be known as well. The general problem of force reconstruction is illustrated in Fig. 1. For a single impact event, if the input position is known in advance, the number of inputs f may be reduced to 1 and thus $\mathbf{h}(t)$ is of the dimension $r \times 1$, so the deconvolution problem is a bit more simplified. Since in practice the impact location is not known, all positions on the structure surface become potential input locations. Depending on the type of model, these locations are usually coinciding with the degrees of Freedom (DOF). For obvious reasons, the number of measurement sensors r is for real world applications normally less than the number of DOFs, so that $r < f$ and the deconvolution problem becomes even more challenging.

Nevertheless, in most practical applications the external loads are not arbitrary distributed in time and space. At least some characteristics about the acting forces are known a priori and should be taken into account in the estimation process. In case of an impact acting on a structure, it is known that the force input is characterized by a short time duration and a spatial concentration. The force history of an impact is mainly defined by the magnitude and the contact duration of the colliding bodies, the latter depends greatly on the stiffness of these bodies. The profile of the force history in the time domain looks approximately like the pulse function shown in Fig. 2. Assuming the shape function $\hat{u}(t)$ of this pulse is known, then the force history of an impact depends only on the pulse width, indicated by the parameter $t_w \in [t_w^{\min}, t_w^{\max}]$, the time $t_m \in [0, t_m^{\max}]$ at which the magnitude is reached and the magnitude value of this pulse $a_{t_m, t_w} \in \mathbb{R}$ itself. Thus, the external force history can be described as function of these parameters: $\hat{u}(t, t_m, t_w) \cdot a_{t_m, t_w}$. The shape function has been normalized so that the magnitude a_{t_m, t_w} becomes a scaling factor of the shape function. Shape functions may either be known from prior experimental investigations or approximated by appropriate impact models (e.g., sinusoidal, Gaussian). However, if the impact is intended to be reconstructed using measured structural responses the parameters are unknown and need to be identified. Additionally the location where the load is applied is unknown as well.

If all potential parameter combinations at an arbitrary force input location j are superimposed, then this equals the actual force input, if all magnitudes a_{t_m, t_w}^j are zero, except the one which belongs to the actual parameter combination (t_w^*, t_m^*) . This can be expressed by means of the Dirac delta function

$$\hat{u}_{\text{sup}}^j(t, t_m, t_w) = \int_0^{t_m^{\max}} \int_{t_w^{\min}}^{t_w^{\max}} \hat{u}^j(t, t_m, t_w) \delta(t_w - t_w^*) \delta(t_m - t_m^*) a_{t_m, t_w}^j dt_w dt_m \quad (3)$$

After discretisation, Eq. (3) becomes

$$\hat{u}_{\text{sup}, k, l, p}^j = \sum_{p=1}^q \sum_{l=0}^m \hat{u}_{k, l, p}^j \Delta_{p^*, p} \Delta_{l^*, l} a_{l, p}^j \quad (4)$$

Here $t_m = l\Delta t$ ($l = 0, 1, 2, \dots, m$) is discretized using the same step size Δt as before in Eq. (2). The discretization of the interval $[t_w^{\min}, t_w^{\max}]$ describing the range of potential impact durations can be thought of as a creation of a sample-force-dictionary which includes a collection of potential impact durations: $t_w^p, (p = 1, 2, \dots, q)$. Now $\Delta_{\bullet, \bullet}$ denotes the Kronecker Delta and p^* and l^* the indices corresponding to the actual parameter combination.

Inserting this force input into the convolution sum Eq. (2) leads to

$$\mathbf{y}_k = \sum_{i=0}^k \mathbf{h}_i \cdot \sum_{l=0}^m \sum_{p=1}^q \hat{\mathbf{u}}_{k-i, l, p} \Delta_{p^*, p} \Delta_{l^*, l} \cdot \mathbf{a}_{l, p} \quad (5)$$

Eq. (5) $\hat{\mathbf{u}}_{k, l, p} \in R^{f \times f}$ is a square matrix containing the normalized force history for the all f potential impact locations, $\mathbf{a}_{l, p} \in R^f$ is the corresponding magnitude vector, which needs to have just one nonzero entry corresponding to the actual input location.

Rewriting this in vector-matrix form leads to

$$\mathbf{Y} = \mathbf{H} \cdot \sum_{p=1}^q \hat{\mathbf{U}}_p \mathbf{A}_p \quad (6)$$

with the measurements $\mathbf{Y} \in R^{r \times n}$, the transfer matrix $\mathbf{H} \in R^{r \times n \times f \cdot n}$, the sample-force-dictionary matrix $\hat{\mathbf{U}}_p \in R^{f \cdot n \times f \cdot m}$ and the magnitude vector $\mathbf{A}_p \in R^{f \times m}$

$$\mathbf{Y} = \begin{bmatrix} \mathbf{y}_0 \\ \mathbf{y}_1 \\ \vdots \\ \mathbf{y}_n \end{bmatrix}, \quad \mathbf{H} = \begin{bmatrix} \mathbf{h}_0 & \mathbf{0} & \cdots & \mathbf{0} \\ \mathbf{h}_1 & \mathbf{h}_0 & \ddots & \vdots \\ \vdots & \vdots & \ddots & \mathbf{0} \\ \mathbf{h}_n & \mathbf{h}_{n-1} & \cdots & \mathbf{h}_0 \end{bmatrix}, \quad \hat{\mathbf{U}}_p = \begin{bmatrix} \hat{\mathbf{u}}_{0,0,p} & \hat{\mathbf{u}}_{0,1,p} & \cdots & \hat{\mathbf{u}}_{0,m,p} \\ \hat{\mathbf{u}}_{1,0,p} & \hat{\mathbf{u}}_{1,1,p} & \ddots & \hat{\mathbf{u}}_{1,m,p} \\ \vdots & \vdots & \ddots & \vdots \\ \hat{\mathbf{u}}_{n,0,p} & \hat{\mathbf{u}}_{n,1,p} & \cdots & \hat{\mathbf{u}}_{n,m,p} \end{bmatrix}, \quad \mathbf{A}_p = \begin{bmatrix} \mathbf{a}_{0,p} \\ \mathbf{a}_{1,p} \\ \vdots \\ \mathbf{a}_{m,p} \end{bmatrix} \quad (7)$$

Due to the properties of the Kronecker Delta and thus to ensure the equivalence of Eqs. (5) and (6), \mathbf{A}_p needs to be the zero vector for $p \neq p^*$. In Addition \mathbf{A}_{p^*} must have just one nonzero element associated with the index l^* .

A further rearrangement of Eq. (6) results in

$$\mathbf{Y} = \mathbf{H} \cdot \underbrace{\begin{bmatrix} \hat{\mathbf{U}}_1 & \hat{\mathbf{U}}_2 & \dots & \hat{\mathbf{U}}_q \end{bmatrix}}_{=: \mathbf{U}} \underbrace{\begin{bmatrix} \mathbf{A}_1 & \mathbf{A}_2 & \dots & \mathbf{A}_q \end{bmatrix}^T}_{=: \mathbf{A}} \quad (8)$$

$$= \mathbf{H} \cdot \mathbf{U} \cdot \mathbf{A} \quad (9)$$

The matrix $\mathbf{U} \in \mathbb{R}^{f \cdot n \times f \cdot m \cdot q}$ contains now all potential impact events in a normalized representation and $\mathbf{A} \in \mathbb{R}^{f \cdot m \cdot q}$ the corresponding magnitudes in a discrete form. The matrix \mathbf{U} may be regarded as entire impact sample-force-dictionary. By multiplying \mathbf{U} with the transfer matrix \mathbf{H} a new transition matrix $\tilde{\mathbf{H}} \in \mathbb{R}^{r \cdot n \times f \cdot m \cdot q}$ is obtained

$$\mathbf{Y} = \tilde{\mathbf{H}} \cdot \mathbf{A} \quad \text{with} \quad \tilde{\mathbf{H}} := \mathbf{H} \cdot \mathbf{U} \quad (10)$$

Impact reconstruction becomes now a problem of solving Eq. (10) for \mathbf{A} . However, it can be easily seen that $\tilde{\mathbf{H}}$ tends to have a lot more columns ($N := f \cdot m \cdot q$) than rows ($M := r \cdot n$). Hence the linear system of equations in Eq. (10) has a lot more unknowns than known and thus solving for \mathbf{A} is in general not possible. But it is known that \mathbf{A} has a very few or even just one nonzero entry and can be considered as sparse vector (see Fig. 3). The property of sparsity of the desired magnitude vector \mathbf{A} is used in the following to obtain an optimal estimate of the impact.

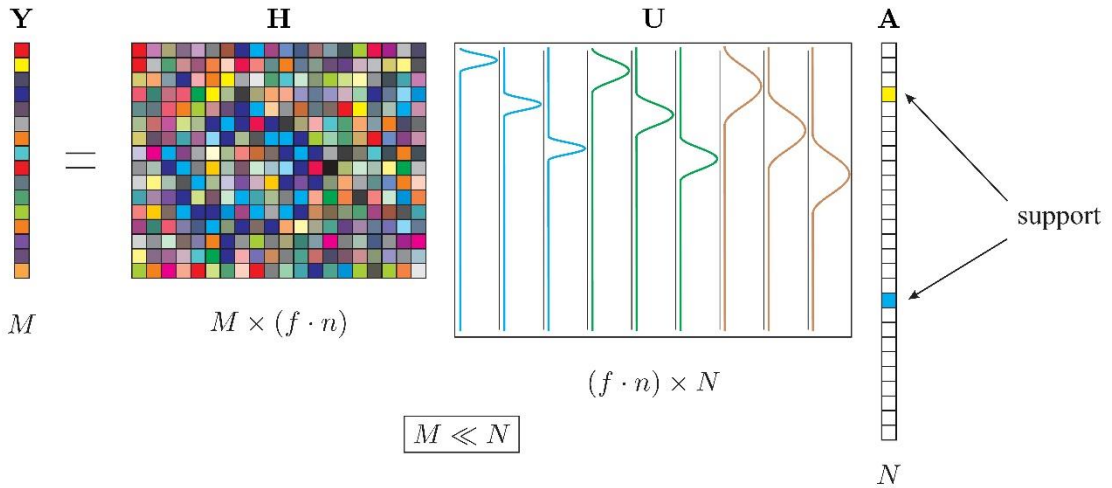


Fig. 3 By pre-multiplying an impact sample-force dictionary, identification becomes a sparse recovery problem

3. Sparse solution

Finding a sparse solution for a high-dimensional underdetermined problem can be thought of an application of Occam's Razor: in face of many possibilities, all of which are plausible, favour the simplest candidate solutions (Gill *et al.* 2011). Here, it can also be regarded as a problem of finding the columns in $\tilde{\mathbf{H}}$ which correlate the most with the measurement vector \mathbf{Y} .

The number of nonzero entries in a vector can be expressed by

$$\|\mathbf{A}\|_0 := |\text{supp}(\mathbf{A})| \quad (11)$$

where $\text{supp}(\mathbf{A}) = \{i : A_i \neq 0\}$ denotes the support of \mathbf{A} . $\|\cdot\|_0$ is frequently referred to as the l_0 -norm, although it is not even a quasi-norm (Fornasier and Rauhut 2011). The most straightforward way to obtain a sparse estimate $\hat{\mathbf{A}}$ for the linear system in Eq. (10) is to minimize the l_0 -norm of the solution vector \mathbf{A}

$$\hat{\mathbf{A}} = \underset{\mathbf{A} \in \mathbb{R}^N}{\text{argmin}} \|\mathbf{A}\|_0 \quad \text{subject to} \quad \mathbf{Y} = \tilde{\mathbf{H}}\mathbf{A} \quad (12)$$

This creates the sparsest solution vector which agrees with the measurements \mathbf{Y} . However the minimization problem in Eq. (12) requires a combinatorial search, making it practically impossible to solve computationally (NP-hard problem). As shown in many other applications (e.g., Donoho (2003) and Donoho (2006)), under the assumption that the solution is sparse, using the l_1 -norm delivers almost the same solution as solving Eq. (12)

$$\hat{\mathbf{A}} = \underset{\mathbf{A} \in \mathbb{R}^N}{\text{argmin}} \|\mathbf{A}\|_1 \quad \text{subject to} \quad \mathbf{Y} = \tilde{\mathbf{H}}\mathbf{A} \quad (13)$$

The l_1 -norm is defined as the sum of the absolute values of \mathbf{A}

$$\|\mathbf{A}\|_1 = \sum_{i=1}^N |A_i| \quad (14)$$

A solution for Eq. (13) can be obtained via linear programming techniques, since l_1 -regularized optimization is a convex problem.

For a measured output vector \mathbf{Y}_ω , the measurement data are usually polluted by some measurement noise $\boldsymbol{\omega}$, so Eq. (10) becomes

$$\mathbf{Y}_\omega = \tilde{\mathbf{H}}\mathbf{A} + \boldsymbol{\omega} \quad (15)$$

In the presence of noise Eq. (13) is in general not capable to deliver a proper estimate of \mathbf{A} , so it needs to be modified to

$$\hat{\mathbf{A}} = \underset{\mathbf{A} \in \mathbb{R}^N}{\text{argmin}} \left\| \mathbf{Y}_\omega - \tilde{\mathbf{H}}\mathbf{A} \right\|_2^2 + \lambda \|\mathbf{A}\|_1 \quad (16)$$

This problem is known as basis pursuit denoising (BPDN) (Chen *et al.* 1998), which is closely related to LASSO regression (Tibshirani 1996). Here, the least-squares minimization is combined with a l_1 -norm which penalizes solutions with numerous nonzero elements. The regularization

parameter λ controls the trade-off between sparsity of the solution and congruence of \mathbf{Y}_ω and $\tilde{\mathbf{H}}\hat{\mathbf{A}}$. λ can be adjusted according to the level of measurement noise ω (Selesnick 2012).

The feasibility of finding a sparse solution via l_1 -minimization has been shown in many applications in recent years. Particularly in the field of Compressive Sensing (CS) the usability of l_1 -minimization attracts a lot of attention (Candès and Wakin 2008, Donoho 2006). Hence, a number of algorithms have been developed to solve Eqs. (13) and (16) (e.g., Berg and Friedlander (2008) and Kim *et al.* (2007)). The one used in this article is the so called *In-Crowd* Algorithm developed by Gill *et al.* (2011). As discussed by Gill, the *In-Crowd* algorithm is one of the fastest solvers for very large sparse problems. The computational complexity of this iterative method is significantly reduced by partially insulating the algorithm from the global problem size and consulting the full dictionary only rarely. A detailed description of the *In-Crowd* Algorithm and its properties can be found in (Gill *et al.* 2011). The following *In-Crowd* optimization procedure has been adopted from there

Step 0) Declare $\hat{\mathbf{A}}$ to be $\mathbf{0}$, so that the residual $\mathbf{r} = \mathbf{Y}_\omega - \tilde{\mathbf{H}}\hat{\mathbf{A}}$ becomes $\mathbf{r} = \mathbf{Y}_\omega$. Additionally, declare the active support set \mathbf{I} to be the empty set.

Step 1) Calculate the “usefulness” $u_j \equiv \left| \langle \mathbf{r}, \tilde{\mathbf{H}}_j \rangle \right| \forall j \in \mathbf{I}^c$, where $\langle \bullet, \bullet \rangle$ denotes the inner product and \mathbf{I}^c the complement of \mathbf{I} .

Step 2) If on \mathbf{I}^c no $u_j > \lambda$, then terminate.

Step 3) Otherwise, add the L components with the largest u_j to \mathbf{I} , but do not add any component for which $u_j \leq \lambda$. Depending on the specific problem, the choice of L will influence the speed of the algorithm, in this study $L = 25$ is set.

Step 4) Solve Eq. (16) exactly on the subspace spanned by all of the components in \mathbf{I} . Use current values of $\hat{\mathbf{A}}$ to warm-start the solver. This subproblem is expected to be dense. For this purpose, Matlab’s built-in *quadprog* function (MathWorks 2011), can be used.

Step 5) Take any zero-valued members of the exact solution of Step 4) out of \mathbf{I} .

Step 6) Set all components of $\hat{\mathbf{A}}$ to be 0 except for the components in \mathbf{I} ; set these to the value found by the exact solution of Step 4).

Step 7) Update $\mathbf{r} = \mathbf{Y}_\omega - \tilde{\mathbf{H}}\hat{\mathbf{A}}$.

Step 8) Go to Step 1).

The so obtained magnitude vector $\hat{\mathbf{A}}$ has just a few nonzero elements and gives directly the information about the impact force history and the impact location. Considering the support of $\hat{\mathbf{A}}$ and its corresponding column in \mathbf{U} the impact location is identified. Moreover, the shape function with the best fit to the actual impact force history is selected. The maximum impact force is stated by the value of the reconstructed nonzero component in $\hat{\mathbf{A}}$.

4. Simulation study

The capability to reconstruct the amplitude and the location of an impact simultaneously from noisy measurements by solving the BPDN problem will be shown first by means of simulation

studies, additionally some properties of the proposed identification process are investigated. For illustration purposes, a uniform simply supported Euler-Bernoulli beam with the properties specified in Fig. 4 is investigated. The structural dynamics of the beam due to an external impact force are described by an analytical model. Throughout all studies (simulation and experiments) the employed structural responses for reconstruction are acceleration measurements. It should be explicitly noted that the shown impact detection method is also applicable for other types of structural models, e.g., finite element or modal models and other types of measurement data (e.g., strain).

4.1 Analytical beam model

In the following a small hint is given how the Markov parameters with appropriate system input positions are obtained for an Euler-Bernoulli beam. A more detailed description can be found in various textbooks. Starting from the equation of motion for a uniform Euler-Bernoulli beam

$$EI_z \frac{\partial^4 w(x,t)}{\partial x^4} + \rho A \frac{\partial^2 w(x,t)}{\partial t^2} = q(x,t) \quad (17)$$

it is assumed that the lateral displacement can be separated in time and space: $w(x,t) = W(x)\zeta(t)$. After a few calculation steps this results in the natural frequency ω_n and the analytical mode shape $W_n(x)$ of the n^{th} mode, $n=1,2,\dots$

$$\omega_n = (n\pi)^2 \sqrt{\frac{EI_z}{\rho AL^4}} \quad \text{and} \quad W_n(x) = \sin\left(\frac{n\pi}{L}x\right) \quad (18)$$

which includes the boundary conditions of the simply supported beam $W(0) = W''(0) = W(L) = W''(L) = 0$. The bending displacement can now be rewritten in modal coordinates $\zeta(t)$ as follows

$$w(x,t) = \sum_{n=1}^{\infty} W_n(x)\zeta_n(t) = \sum_{n=1}^{\infty} \sin\left(\frac{n\pi}{L}x\right)\zeta_n(t) \quad (19)$$

A state space representation can be obtained from Eqs. (17) and (19)

$$\dot{\mathbf{x}}(t) = \Phi \mathbf{x}(t) + \mathbf{B} \mathbf{u}(t) \quad (20a)$$

$$\mathbf{y}(t) = \mathbf{C} \mathbf{x}(t) + \mathbf{D} \mathbf{u}(t) \quad (20b)$$

with the state equation Eq. (20(a)) and the output or measurement equation Eq. (20(b)). By adding proportional modal damping $2\xi_n \omega_n \dot{\zeta}(t)$ the state equation Eq. (20(a)) can be written for a finite number of modes $n=1,2,\dots,k$

$$\dot{\mathbf{x}}_{2k \times 1}(t) = \begin{bmatrix} \dot{\zeta}_{k \times 1} \\ \ddot{\zeta}_{k \times 1} \end{bmatrix} = \begin{bmatrix} \mathbf{0}_{k \times k} & \mathbf{I}_{k \times k} \\ -\mathbf{\Omega}_{k \times k}^2 & (-2\mathbf{Z}\mathbf{\Omega})_{k \times k} \end{bmatrix} \begin{bmatrix} \zeta_{k \times 1}(t) \\ \dot{\zeta}_{k \times 1}(t) \end{bmatrix} + \begin{bmatrix} \mathbf{0}_{k \times m} \\ \left(\frac{2}{\rho AL} \left[\int_0^L U_i(x) W_n(x) dx \right] \right)_{k \times m} \end{bmatrix} \begin{bmatrix} u_1(t) \\ \vdots \\ u_m(t) \end{bmatrix}_{m \times 1} \quad (21)$$

In Eq. (21), the external force is separated into m forces and in time and space: $q(x,t) = \sum_{i=1}^m q_i(x,t) = \sum_{i=1}^m U_i(x)u_i(t)$. For a spatially concentrated force the space allocation $U_i(x)$ can be expressed by means of Dirac's delta function $\delta: U_i(x) = \delta(x - s_i)$, where s_i denotes the points of applied force and $i=1,2,\dots,m$ the number of concentrated forces. Moreover, $\mathbf{\Omega}$ and \mathbf{Z} are the diagonal matrices of the natural frequencies and modal dampings. The individual terms of Eq. (21) can be assigned to the corresponding vectors or matrices of Eq. (20(a)).

With the help of Eq. (19) as second time derivative $\ddot{w}(x,t) = \sum_{n=1}^k W_n(x)\ddot{\zeta}_n(t)$, the output equation Eq. (20(b)) for r accelerometers becomes

$$\begin{aligned} \begin{bmatrix} \ddot{w}_1(x_1,t) \\ \vdots \\ \ddot{w}_r(x_r,t) \end{bmatrix} &= \begin{bmatrix} -\omega_1^2 W_1(x_1) & \cdots & -\omega_k^2 W_k(x_1) \\ \vdots & \ddots & \vdots \\ -\omega_k^2 W_k(x_r) & \cdots & -\omega_k^2 W_k(x_r) \end{bmatrix} \begin{bmatrix} \zeta_1(t) \\ \vdots \\ \zeta_k(t) \end{bmatrix} \\ &+ \begin{bmatrix} -2\zeta_1 \omega_1 W_1(x_1) & \cdots & -2\zeta_k \omega_k W_k(x_1) \\ \vdots & \ddots & \vdots \\ -2\zeta_1 \omega_1 W_1(x_r) & \cdots & -2\zeta_k \omega_k W_k(x_r) \end{bmatrix} \begin{bmatrix} \dot{\zeta}_1(t) \\ \vdots \\ \dot{\zeta}_k(t) \end{bmatrix} \\ &+ \begin{bmatrix} \sum_{n=1}^k p_{1n} W_n(x_1) & \cdots & \sum_{n=1}^k p_{mn} W_n(x_1) \\ \vdots & \ddots & \vdots \\ \sum_{n=1}^k p_{1n} W_n(x_r) & \cdots & \sum_{n=1}^k p_{mn} W_n(x_r) \end{bmatrix} \begin{bmatrix} u_1(t) \\ \vdots \\ u_m(t) \end{bmatrix} \end{aligned} \quad (22)$$

where x_i represents the i^{th} sensor position along the beam and $p_{in} = \frac{2}{\rho AL} \sin\left(\frac{n\pi}{L} s_i\right)$ includes the projection of the spatial load distribution onto the n^{th} mode shape. The first two elements on the right hand side of Eq. (22) can be combined into the \mathbf{C} matrix of Eq. (20(b)) and the last term is associated with the \mathbf{D} matrix. Since, the impact location is unknown in advance some potential input positions along the beam need to be predefined (e.g., red dots in Fig. 4), in order to obtain appropriate matrices \mathbf{B} and \mathbf{D} . No input positions are predefined directly at the bearings, as an impact applied at this location won't cause any beam vibration and is therefore undetectable for vibration based force reconstruction methods.

For the simulation study as well as for the experimental investigation it is necessary to convert the continuous state space model of Eq. (20) into a discret-time state space system

$$\mathbf{x}_{k+1} = \mathbf{\Phi}_D \mathbf{x}_k + \mathbf{B}_D \mathbf{u}_k \quad (23a)$$

$$\mathbf{y}_k = \mathbf{C} \mathbf{x}_k + \mathbf{D} \mathbf{u}_k \quad (23b)$$

The state space representation of the analytical beam allows us now to determine the Markov parameters (Smith 2007) as follows

$$\mathbf{h}_0 = \mathbf{D} \quad , \quad \mathbf{h}_n = \mathbf{C}(\mathbf{\Phi}_D)^{n-1} \mathbf{B}_D \quad (24)$$

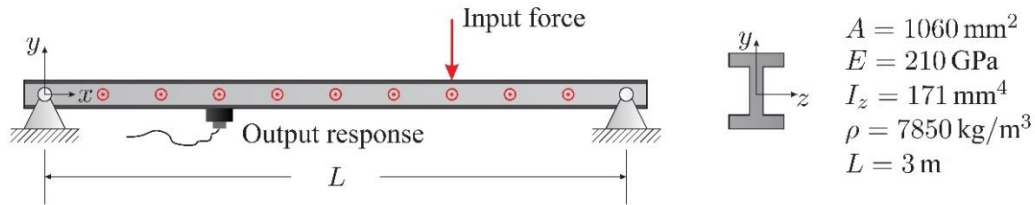


Fig. 4 Uniform simply supported beam

4.2 Simulation results

The vibrations of the simply supported beam due to an impact event are simulated with MATLAB®. Here the structural model from section 4.1 is used. In order to simulate an impact event as input to the simulation model, but also to create a sample-impact-dictionary, a shape function needs to be defined. The shape function of the impact force history is commonly modelled as half or quarter cycle-sine pulses (see e.g., Grady 1988 and Yan and Zhou 2009)

$$\hat{u}(t, \zeta, \Delta) = \begin{cases} \sin\left(\frac{\pi(t - \zeta + \Delta/2)}{\Delta}\right), & \text{if } \zeta - \frac{\Delta}{2} < t < \zeta + \frac{\Delta}{2} \\ 0, & \text{otherwise} \end{cases} \quad (25)$$

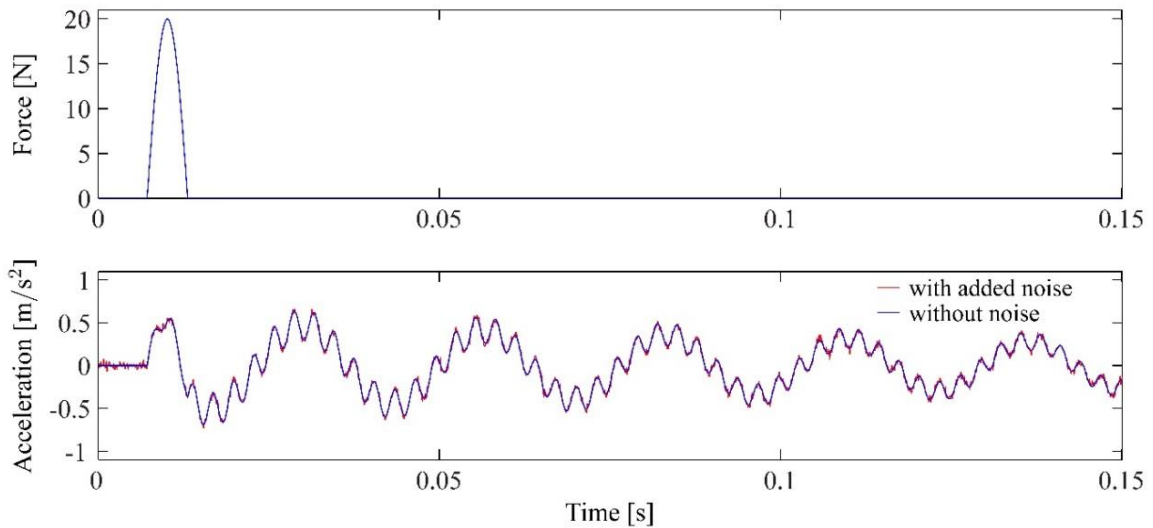


Fig. 5 Top: Simulated Impact applied at normalized beam position 0.6, Bottom: Simulated acceleration data at normalized beam position 0.5

As before, the impact duration is indicated by Δ , which in this case equals the contact duration of the colliding bodies and ξ is the time when the maximum force occurs. However, different shape functions are possible; e.g., Hann function, Gaussian function, but also various types of asymmetric shape functions.

This so formed normalized impact force is multiplied by a certain magnitude a_{true} and applied at a position s_{true} along the beam. White Gaussian noise with a standard deviation of three percent of the maximum measurement value is added to the simulated outputs to imitate real acceleration measurement data. For the first simulation three outputs are generated at the normalized beam length 0.4, 0.5 and 0.65 (in the remainder of this paper all beam positions will be given in normalized beam length). The influence of the sensor placement and measurement noise is discussed later. The structural model used for simulating the measurement data and for reconstructing the impact is identical. It consisted of the first four modes so that with the given properties, beam vibrations up to 600 Hz can be captured. The required force input positions of the reconstruction model are placed equidistantly along the beam with $\Delta x/L = 0.05$. The maximum possible spatial resolution of these points depends greatly on the number of modes used in the structural model respectively the accuracy of the model used. The simulation result with and without measurement noise for acceleration output at point $x/L = 0.5$ due to an impact at beam position $x/L = 0.6$ can be seen in Fig. 5.

For the first studies the width of the shape function Δ_{true} is assumed to be known, as may be the case if specific information about the colliding bodies and their contact behaviour is available, e.g. from preliminary investigations. Therefore, the sample-impact-dictionary is composed of one type of pulse function ($q = 1$). The reconstruction result of an impact applied on one of the predefined force input position at $x/L = 0.6$ is shown in Fig. 6. On the right hand side the exact and the identified force history for the true impact location are shown. In order to take the effect of randomness of the measurement noise into account, one hundred simulations with identical simulation properties are performed. The mean magnitude estimation error is determined as 1.6274% with a standard deviation of 0.0223%. The left plot displays spatial load distribution along the beam for the moment in time of maximum force. It can be seen that the impact location is detected as well. The mean localization error reads as 4.4×10^{-4} .

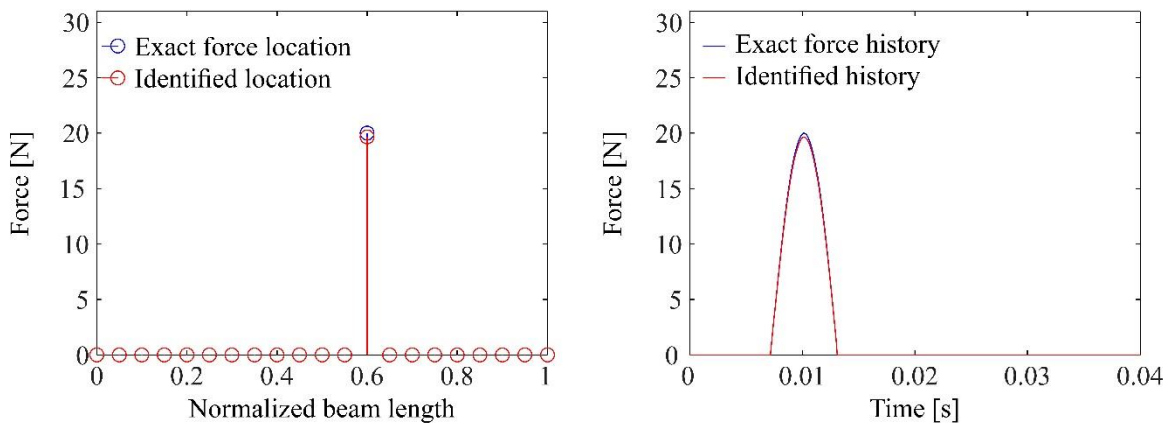


Fig. 6 Impact reconstruction results (left: spatial load distribution, right: force time history)

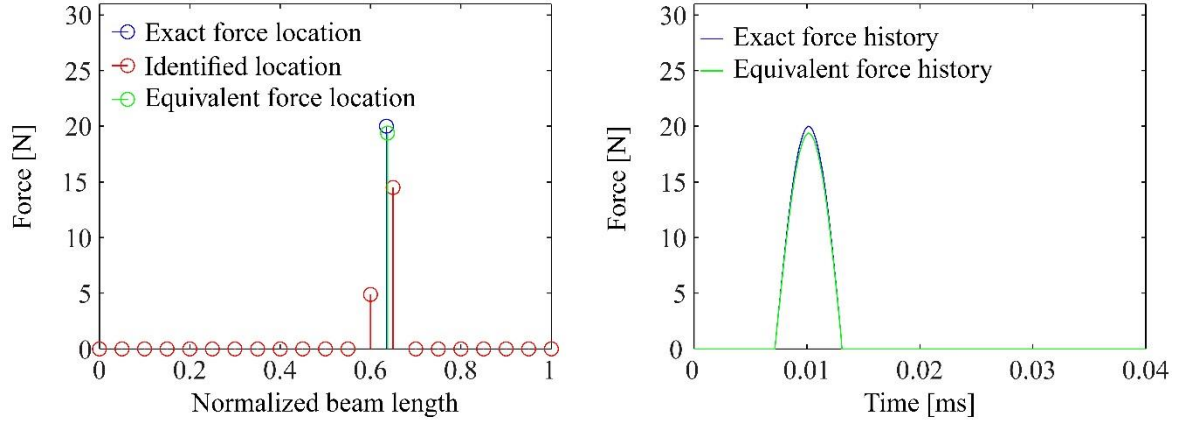


Fig. 7 Equivalent force reconstruction results (left: spatial load distribution, right: force time history)

Even in cases when the impact is not located at one of the predefined force input positions, the location can be identified. A simulation result for an impact applied on beam position $x/L = 0.635$ (divergent from predefined positions) can be seen in Fig. 7. As shown, the total impact at the exact position s_{true} is divided to the neighbouring force input positions s_i and s_{i+1} of the employed reconstruction model. So the reconstruction algorithm identifies, as the sparsest solution to the minimization problem, forces at the model input positions next to the true one (red bars in Fig. 7).

In order to identify the true impact location and magnitude, the reconstructed forces need to be combined to an equivalent force. The magnitude of an equivalent force is simply the sum of the reconstructed magnitudes $\hat{a}_{\text{true}} = a_{i+1} + a_i$ and by considering the equilibrium of moments for these magnitude values, the position of the equivalent force can be localized

$$\hat{s}_{\text{true}} = s_{i+1} - \frac{a_i}{a_{i+1} + a_i} \cdot (s_{i+1} - s_i) \quad (26)$$

The green graph in Fig. 7 illustrates the identified force history and the estimated impact location for the equivalent force. Here the mean magnitude estimation error is 3.02% and the mean localization error 2.4×10^{-3} .

4.3 Sensitivity studies

Now the question may arise, how the reconstruction accuracy varies, if no prior information about the shape function is available and none of the impact shapes in the sample-dictionary matches the true impact shape. Therefore, several simulation studies using deviating impact shapes are carried out. In each case $q = 1$ still applies. The deviation of the shape function is introduced by a variation of the impact durations. The actual impact duration is indicated by Δ_{true} and the one used in the sample-dictionary by Δ_{used} . Fig. 8 displays the estimation error for deviation of

the shape function of $\pm 20\%$, on the right hand side the absolute localization error given in normalized beam length and on the left hand side the relative error of the force history and the estimated magnitude

$$\delta_{\text{history}} := \sqrt{\frac{\|u_{\text{true}} - u_{\text{estimated}}\|_2^2}{\|u_{\text{true}}\|_2^2}} ; \quad \delta_{\text{mag}} := \frac{a_{\text{true}} - a_{\text{estimated}}}{a_{\text{true}}} \quad (27)$$

Where u_{true} and $u_{\text{estimated}}$ are the exact and the estimated force history vectors for the true and the identified impact location, a_{true} and $a_{\text{estimated}}$ are the corresponding magnitude values. Small deviation of the assumed pulse width may lead to greater errors of the force history. However, for a lot of impact identification applications the maximum force occurring is the critical value and of more interest. As Fig. 8 indicates the estimate of impact magnitude and impact location are not sensitive to deviations of sample-impact dictionary and actual impact. Fig. 9 illustrates the force history estimation results for two different impulse duration dictionaries and explains the different error curves in the left plot of Fig. 8.

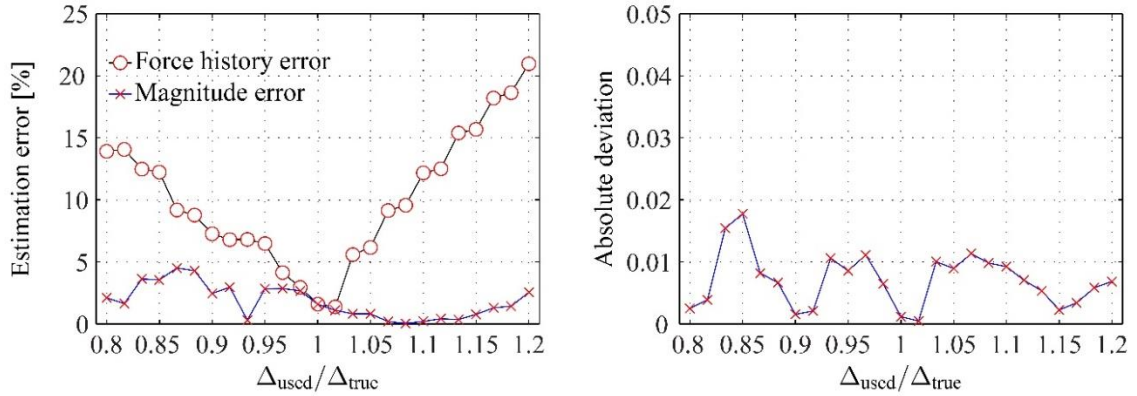


Fig. 8 Effect of shape function deviation on the reconstruction accuracy (left: relative error of magnitude and time history estimation, right: deviation from actual normalized location)

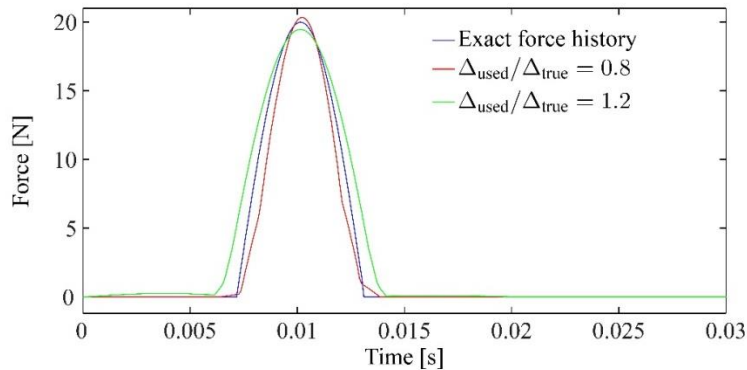


Fig. 9 Time history for reconstruction using deviating shape functions

Although the presented reconstruction methodology is able to compensate measurement noise, the level of noise may have an influence on the reconstruction accuracy. In addition, different sensor networks might affect the identification result. In the following these influences are investigated.

So far, all studies are run with an added simulated measurement noise, the noise level is set by the standard deviation σ of the Gaussian noise, which is chosen to be three percent of the maximum measurement value. As mentioned before the regularization parameter λ has to be adjusted to this noise level. Setting λ larger leads to a more regularized solution of Eq. (16) and makes the estimation less sensitive to noise, but this yields more attenuation of the reconstructed force history, contrariwise yields a smaller chosen λ (less regularization) to more noise sensitivity but less attenuation (Gill *et al.* 2011). Because, the time history of the noise is not known, it is reasonable to use the statistical information of the noise to adjust λ . In the simulation studies, it has turned out, that a proper way of setting λ is according to the standard deviation: $\lambda = 10\sigma$.

The effect of noise to the identification accuracy of impact size and impact location is shown in Fig. 10. The resulting error is displayed for a raising standard deviation of the measurement noise from 1 to 20 percent of the maximum measurement value. As expected, an increasing measurement noise leads to a larger deviation between true and estimated magnitude. However, the estimate of impact location is largely independent of the noise which implies that the support of \mathbf{A} can be determined very reliably.

The inaccuracies of the reconstruction result due to large measurement noise and deviations in the sample-impact-dictionary may be compensated by using a different sensor setup. In the following, several simulation studies are carried out, in order to determine the influence of the sensor setup. Therefore, the number of accelerometers is increased from just one sensor up to 10 measurement positions along the beam. To isolate the influence of sensor setup and to ensure independence from other sources of interference, the sample-impact-dictionary contains the true impact and the level of noise is kept constant at a level of 3 percent of the maximal measurement value. By increasing the number of accelerometers the sensors are added at different beam positions in the following order:

These positions are chosen considering the mode shapes identified in 4.1 and their vibration nodes to obtain optimum signal to noise ratio (SNR). Moreover, it is ensured that the sensors are not arranged symmetrically to avoid redundant information. The resulting errors for impact estimation magnitude and for localization for the different setups are shown in Fig. 11. It shows that with only two sensors satisfactory impact identification may be possible. However, even with just one sensor the proposed reconstruction algorithm is able to make a statement of the impact location. The deviation of impact magnitude is larger in this case, but a rough estimation of the force history can still be given.

Table 1 Order of sensor placement, the position is described in normalized beam length

Sensor	1	2	3	4	5	6	7	8	9	10
Position	0.4	0.65	0.5	0.31	0.725	0.45	0.2	0.81	0.15	0.93

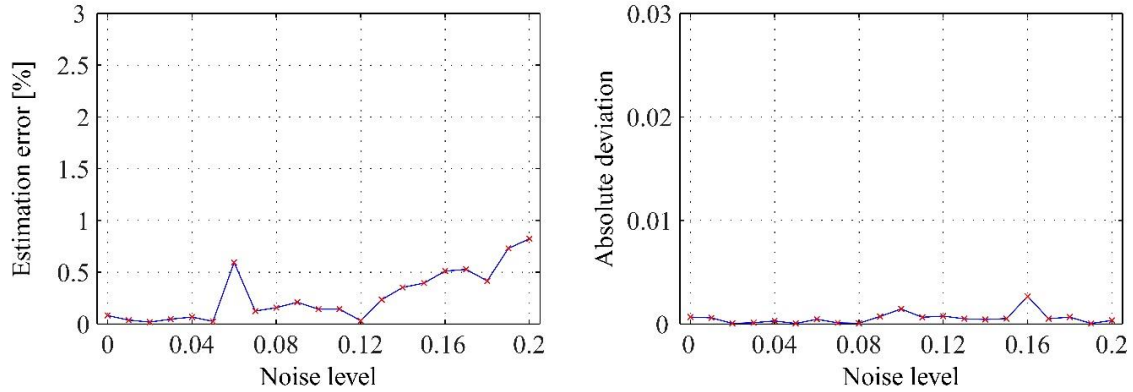


Fig. 10 Effect of measurement noise level on the reconstruction accuracy (left: relative error of magnitude estimation, right: deviation from actual normalized location)

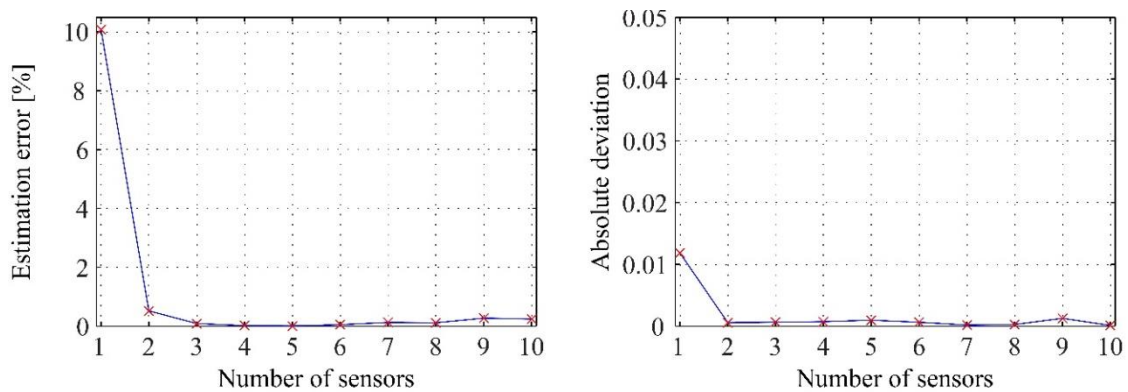


Fig. 11 Effect of the sensor number to the reconstruction accuracy (left: relative error of magnitude estimation, right: deviation from actual normalized location)

5. Experiment

For experimental validation of the presented impact identification strategy an experimental test bench similar to the simulation model is set up. A beam of $L = 3$ m length with the same properties specified in Fig. 4 is placed onto two support blocks (see Fig. 12(d)). These supports are rigidly attached to the floor in a guide rail. Five piezoelectric accelerometers (Fig. 12(a)) are mounted on the beam bottom side. The sensors are placed at positions 0.13, 0.36, 0.5, 0.73, 0.83 of the normalized beam length. The beam structure is excited by an impact with an impulse force hammer (Fig. 12(b)). The built-in force sensor is able to measure the force history applied by the hammer, which is used later to confirm the reconstructed impact load. The impulse hammer has a hard rubber tip to excite frequencies up to 500 Hz, which covers the first four natural frequencies of the beam. The sampling time for acquiring of measurement data throughout all experimental investigations is 0.1 ms. These data are filtered by a 100Hz analog low-pass filter (Fig. 12(c)).

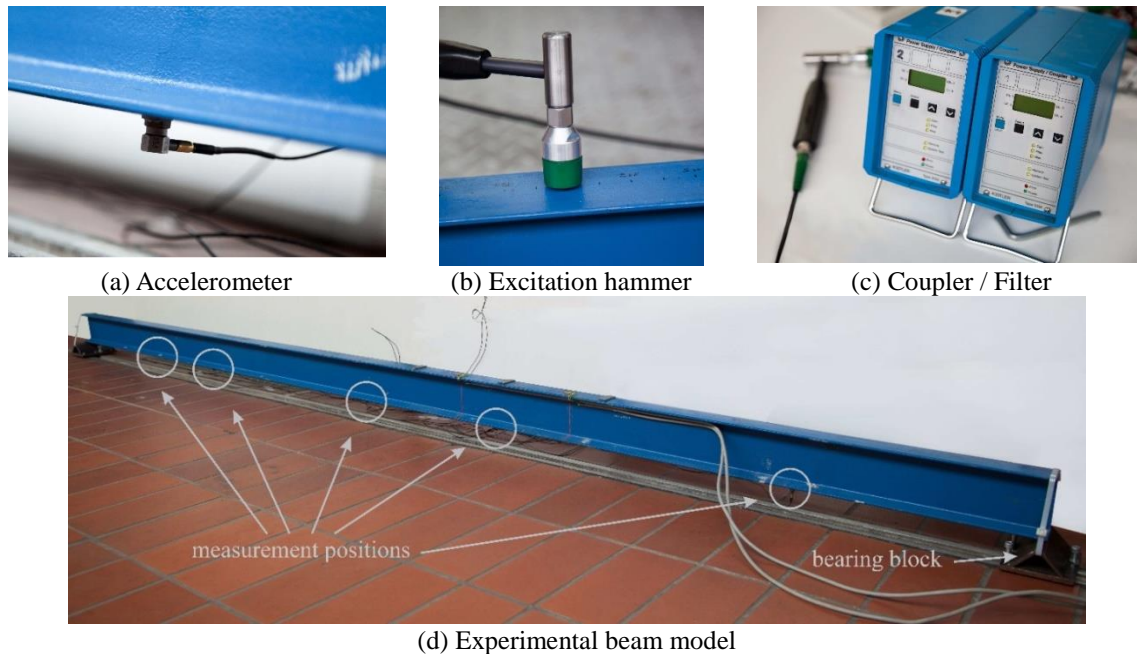


Fig. 12 Experimental study on beam model

The analogy of the test bench to the simulation model allows the use of the same structural model. The force application points defined in this model are set every 0.3 m, which equals a distance of 0.1 normalized beam length. The during the first investigations employed sample-impact-force-dictionary contains five sinus shaped impacts with different pulse widths, so that $q=5$ applies. In addition, only two of the five sensor signals (at positions 0.5 and 0.73) are used for the impact identification process. Fig. 13 shows the reconstruction results for an impact applied at $x/L=2/3$. The deviation of the calculated impact location amounts $\Delta x/L=0.0065$ which corresponds to an absolute value of 1.94 cm. In assessing the localization accuracy, the hammer tip with a width of 2cm (see Fig. 12(b)) needs to be considered. The magnitude estimation error amounts in this case 8.26%.

For a second experimental investigation several force time histories are recorded with the impulse force hammer in a preliminary study. Here three different hammer tips with varying stiffness are used. By means of the obtained data an improved sample-impact-dictionary is set up. In this dictionary each hammer tip corresponds to a certain pulse width or impact shape, thus $q=3$ applies. Also in this case only the previous two accelerometers are employed. The reconstruction results are show in Fig. 14. Now the magnitude estimation error can be decreased to 3.93%. The localization error slightly increases to $\Delta x/L=0.008$, which equals 2.4 cm respectively. With such kind of "trained" sample-dictionary, it is even possible to directly identify the properties of the colliding body, by just considering the supports of the reconstructed vector. Here this means, that the used hammer tip is identified, without requiring a subsequently frequency analyses of the estimated force history.

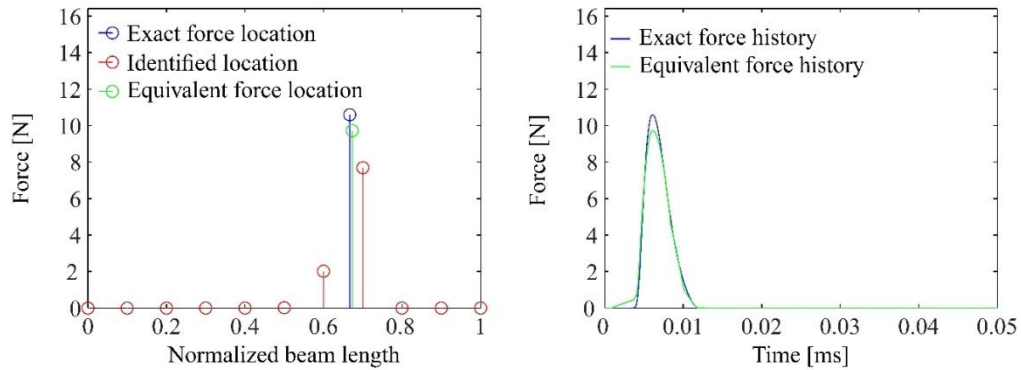


Fig. 13 Experimental reconstruction results for sinus shape sample-impact-dictionary

The experimental investigations have shown furthermore that divergent from the analytical structural model the bearings are not perfectly rigid and some vibrations at the beam edges can be observed, which is not consistent with the assumption of a rigid support. By implication, impacts applied at the bearings will in this case also cause some vibrations, which is also not consistent with the employed structural beam model. This modelling error also has an influence on the detection accuracy of impact applied close to the ends of the beam. In these cases the impact locations are estimated closer to the beam middle area.

6. Conclusions

In this paper the problem of reconstructing an impact from structural responses is addressed. In order to overcome the ill-posed inverse problem of impact identification, the specific characteristics of an impact event are employed. Thus the reconstruction problem can be transformed in sparse recovery issue of the linear system of equations, which can be tackled by the so called basis pursuit denoising approach.

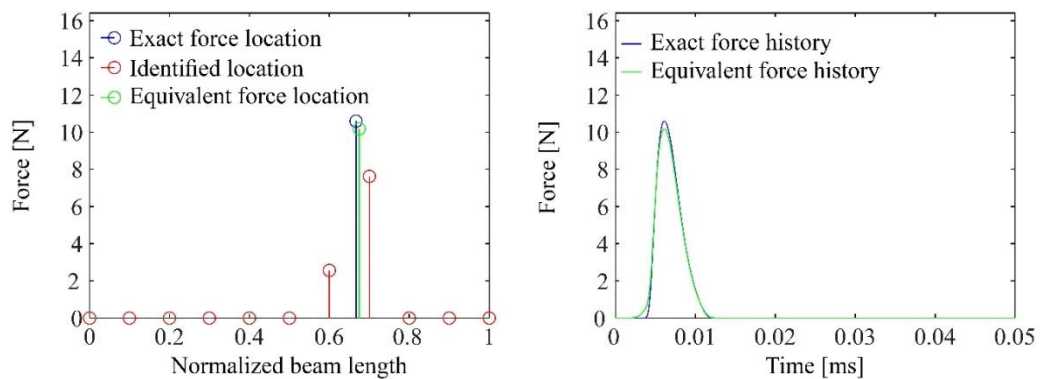


Fig. 14 Experimental reconstruction results for experimentally determined sample-impact-dictionary

It has been shown that the proposed impact identification method is able to reconstruct the impact location and the impact force history, simultaneously. By means of simulations studies and experimental investigations it has been demonstrated that this method is capable to operate even in the presence of very noisy measurement data. Especially the estimation of the impact location and the impact magnitude turned out to be very robust, also against errors of the prior assumed impact force history shape functions and noise.

The number of required sensors is significant less compared to other identification methods, which are able to estimate simultaneously the location the magnitude. For the investigated beam structure two accelerometers are sufficient to obtain satisfying estimates. Furthermore, the simulation study has shown that by employing very accurate models only a single accelerometer is required for impact detection, although the deviations are larger in this case. Even in the case of bigger differences of the structural model, a slight increase of the sensor number is able to compensate these deviations.

The proposed sparse identification method opens up a lot of new opportunity in the field of load reconstruction. The idea of employing prior knowledge of the force characteristics to create a sparse problem is transferable to other load reconstruction tasks, e.g., identification of harmonic excitation. The discussed advantages make it interesting to extend this method to this end particularly with regard to reduce the number of required sensors.

References

- Abrate, S. (2005), *Impact on Composite Structures*, Cambridge University Press, Cambridge, United Kingdom.
- Candès, E. and Wakin, M. (2008), "An introduction to compressive sampling", *IEEE Signal Pr. Magazine*, **25**(2), 21-30.
- Chang, C. and Sun, C. (1989), "Determining transverse impact force on a composite laminate by signal deconvolution", *Exper. Mech.*, **29**(4), 414-419.
- Chen, S., Donoho, D. and Saunders, M. (1998), "Atomic decomposition by basis pursuit", *SIAM J. Scientific Comput.*, **20**(1), 33-61.
- Donoho, D.L. (2006), "Compressed sensing", *IEEE T. Inform. Theory*, **52**(4), 1289-1306.
- Donoho, D.L. and Elad, M. (2003), "Optimally sparse representation in general (nonorthogonal) dictionaries via l_1 minimization", *Proceeding of the National Academy of Sciences*, **100**(5), 2197-2202.
- Donoho, D.L. and Huo, X. (2006), "Uncertainty principles and ideal atomic decomposition", *IEEE T. Inform. Theory*, **47**(7), 2845-2862.
- Doyle, J. (1984), "An experimental method for determining the dynamic contact law", *Exper. Mech.*, **24**(1), 10-16.
- Fornasier, M. and Rauhut, H. (2011), "Compressive sensing", In O. Scherzer, editor, *Handbook of Mathematical Methods in Imaging*, pages, Springer New York, 187-228.
- Gaul, L. and Hurlbauss, S. (1998), "Identification of the impact location on a plate using wavelets", *Mech.l Syst. Signal Pr.*, **12**(6), 783-795.
- Gill, P., Wang, A. and Molnar, A. (2011), "The in-crowd algorithm for fast basis pursuit denoising", *IEEE T. Signal Pr.*, **59**(10), 4595-4605.
- Ginsberg, D. and Fritzen, C.P. (2014), "New approach for impact detection by finding sparse solution", *Proceedings of the International Conference on Noise and Vibration Engineering (ISMA2014)*, 2051-2064.
- Grady, J. (1988), "Contact force history and dynamic response due to the impact of a soft projectile"
- Inoue, H., Harrigan, J.J. and Reid, S.R. (2001), "Review of inverse analysis for indirect measurement of

- impact force”, *Appl. Mech. Rev.*, **54**(6), 503-524.
- Jacquelin, E., Bennani, A. and Hamelin, P. (2003), “Force reconstruction: analysis and regularization of a deconvolution problem”, *J. Sound Vib.*, **265**(1), 81-107.
- Jones, R.T., Sirkis, J.S. and Friebele, E.J. (1997), “Detection of impact location and magnitude for isotropic plates using neural networks”, *J. Intel. Mat. Syst. Str.*, **8**(1), 90-99.
- Kim, S.J., Koh, K., Lustig, M., Boyd, S. and Gorinevsky D. (2007), “An interior-point method for large-scale ℓ_1 -regularized least squares”, *IEEE J. Selected Topics in Signal Pr.*, **1**(4), 606-617.
- Klinkov, M. and Fritzen, C.P. (2007), “An updated comparison of the force reconstruction methods”, *Key Eng. Mater.*, **347**, 461-466.
- Li, H.N., Yi, T.H., Ren, L., Li, D.S. and Huo, L.S. (2014), “Reviews on innovations and applications in structural health monitoring for infrastructures”, *Struct. Monit. Maint.*, **1**(1), 1-45.
- MathWorks (2011), Quadratic Programming: Optimization Algorithms and Examples (Optimization Toolbox).
- Park, J., Ha, S. and Chang, F.K. (2009), “Monitoring impact events using a system-identification method”, *AIAA J.*, **47**(9), 2011-2021.
- Selesnick, I. (2012), *Sparse deconvolution (an mm algorithm)*, Technical report, Polytechnic Institute of New York University, October.
- Smith, J. O. (2007), *Introduction to Digital Filters with Audio Applications*, W3K Publishing.
- Stevens, K. (1987), “Force identification problems –an overview”, *Proceedings of SEM*, Houston, USA.
- Tibshirani, R. (1996), “Regression shrinkage and selection via the lasso”, *J. Royal Statistical Society (Series B)*, **58**, 267-288.
- Torres-Arredondo, M.A. and Fritzen, C.P. (2012), “Impact Monitoring in smart structures based on Gaussian processes”, *Proceedings of the 4th International Symposium on NDT in Aerospace*, Augsburg, Germany, November.
- van den Berg, E. and Friedlander, M.P. (2008), “Probing the pareto frontier for basis pursuit solutions”, *SIAM J. Sci. Comput.*, **31**(2), 890-912.
- Yan, G. and Zhou, L. (2009), “Impact load identification of composite structure using genetic algorithms”, *J. Sound Vib.*, **319**(3-5), 869-884.